CARBON 47 (2009) 1297–1302

available at www.sciencedirect.com

ScienceDirect

journal homepage: www.elsevier.com/locate/carbon

Density measurement of size selected multiwalled carbon nanotubes by mobility-mass characterization

S.H. Kim[1], *G.W. Mulholland*, *M.R. Zachariah*[*]

Departments of Mechanical Engineering and Chemistry and Biochemistry, University of Maryland, College Park, MD 20742, USA
National Institute of Standards and Technology, Gaithersburg, MD 20899, USA

ARTICLE INFO

Article history:
Received 5 September 2008
Accepted 8 January 2009
Available online 14 January 2009

ABSTRACT

We employ a combination of gas phase particle mobility and mass methods to make the first absolute density measurement of gas phase grown carbon nanotubes (CNTs). The approach combines a tandem differential mobility analyzer and aerosol particle mass analyzer in series to achieve two steps of electrical mobility classifications of the CNTs and one of mass classification. In the first mobility classification step a stream of monodisperse catalytic particles was produced by pulsed laser ablation. These mobility-classified catalysts seeded the aerosol growth of CNTs, where were directly passed to a second electrical mobility classification step which allows classification of the diameter-controlled CNTs in length. These diameter- and length-classified CNTs were finally introduced into the aerosol particle mass analyzer to measure their mass distribution. We found that the condensed phase density of CNTs was 1.74 ± 0.16 g/cm^3 for two different groups of CNTs with diameters of ~15 and ~22 nm. This value is lower (about 3 sigma) than for graphite, and about 1 sigma lower than the average value for density measurements for carbon black.

1. Introduction

This paper describes what we believe to be the first measurements of the density of multiwalled carbon nanotubes (CNTs). Our density corresponds to the condensed phase density of the CNTs and is based on measurements of the mass and volume of the nanotubes in an aerosol form. These measurements are made on nanotubes that all have essentially the same diameter and length. The ability to generate such nanotubes is an essential feature of the experiment. In this approach, we employ the differential mobility analyzer (DMA) and the aerosol particle mass analyzer (APM) in series to measurement the volume and mass of CNTs on-the-fly. The density of CNTs is obtained by taking the ratio of measured mass to volume.

2. Experimental

This approach was in part inspired by the study by Park et al. [1], who measured the condensed phase density of fractal-like diesel agglomerates consisting of spherical primary particles. While the structure of a CNT is much different than a soot agglomerate, in both cases there is a similar relationship between the projected area of the particle and its electrical mobility. This relationship is key to the analysis.

The volume of the nanotube is obtained using a DMA, which is widely used in characterizing the size distribution

[*] *Corresponding author:* Address: Departments of Mechanical Engineering and Chemistry and Biochemistry, University of Maryland, College Park, MD 20742, USA. Fax: +1 3013149477.
E-mail address: mrz@umd.edu (M.R. Zachariah).

[1] Present address: Department of Nanosystem and Nanoprocess Engineering, Pusan National University, Korea.

0008-6223/$ - see front matter
doi:10.1016/j.carbon.2009.01.011

of aerosols (Kim et al. [2]). Here we include a brief description of the salient features of the mobility classifier. The DMA consists of two coaxial electrodes with a flow in the axial direction and the electric field in the radial direction. The primarily singly charged CNTs enter near the outer electrode (see Fig. 1) and move toward the center electrode as it flows through the instrument. Some of the charged aerosol exits through a slit in the center electrode. The inlet aerosol flow is small compared to sheath flow, Q_c, and the aerosol flow exiting the DMA is equal to the aerosol flow into the DMA. For a given voltage, the mean electric mobility Z_m of the aerosol exiting through the slit in the center electrode of the DMA is given by Knutson and Whitby [3]:

$$Z_m = \frac{Q_c \ln(r_2/r_1)}{2\pi V_{DMA} L_{DMA}}, \quad (1)$$

where V_{DMA} is the potential difference between the electrodes and r_1, r_2, and L_{DMA} are the inner and outer radii of the annular region and L_{DMA} the distance between the aerosol inlet and outlet.

Using Dahneke's expression for the drag force on a cylinder in the free molecular limit, one obtains the following relationship between the projected area of a randomly oriented, singly charged cylinder and its mobility using the method we have previously developed (Kim et al. [4]):

$$A_{p,cyl} = L_{CNT} D_{CNT} = \frac{0.326 e \lambda}{\mu Z_p}, \quad (2)$$

where e is the elementary electrical charge, λ is the mean free path of gas, and μ is the gas viscosity, and L_{CNT} and D_{CNT} are the length and diameter of CNT. In this analysis it is assumed that 90% of the gas collisions are diffuse and 10% specular. This inverse relationship between projected area and electrical mobility in the free molecular limit is also obtained for spheres and soot agglomerates with fractal dimension less than two [1]. The flow regime for a cylinder is set by the diameter and the Knudsen number ($2\lambda/D_{CNT}$) for the 15 and 22 nm CNTs, about 9 and 6, are on the free molecular limit side of the transition from continuum to free molecular.

To validate this expression, projected area measurements were made using both the DMA and then TEM analysis of particles passing through the DMA at the peak in the mobility distribution. The following linear relation was obtained between the projected area measured by TEM analysis, A_{pCNT}, and the projected area based on the DMA measurements (Eq. (2)) of 15 nm CNTs with lengths of 130, 260, 540, and 1200 nm:

$$A_{pCNT} = C_1 A_{p,DMA} + C_2 \quad (3)$$

where, $C_1 = 1.8071$ and $C_2 = -1676.1\ \text{nm}^2$. The estimated uncertainty in the value of A_{pCNT} is ±7.1% based on uncertainties of 5% for TEM analysis of the diameter and length of the CNT. The nonzero value of C_2 and C_1 not being one are a result of the partial alignment of the CNT (Kim et al. [4,5]) in the electric field and of not being fully in the free molecular regime.

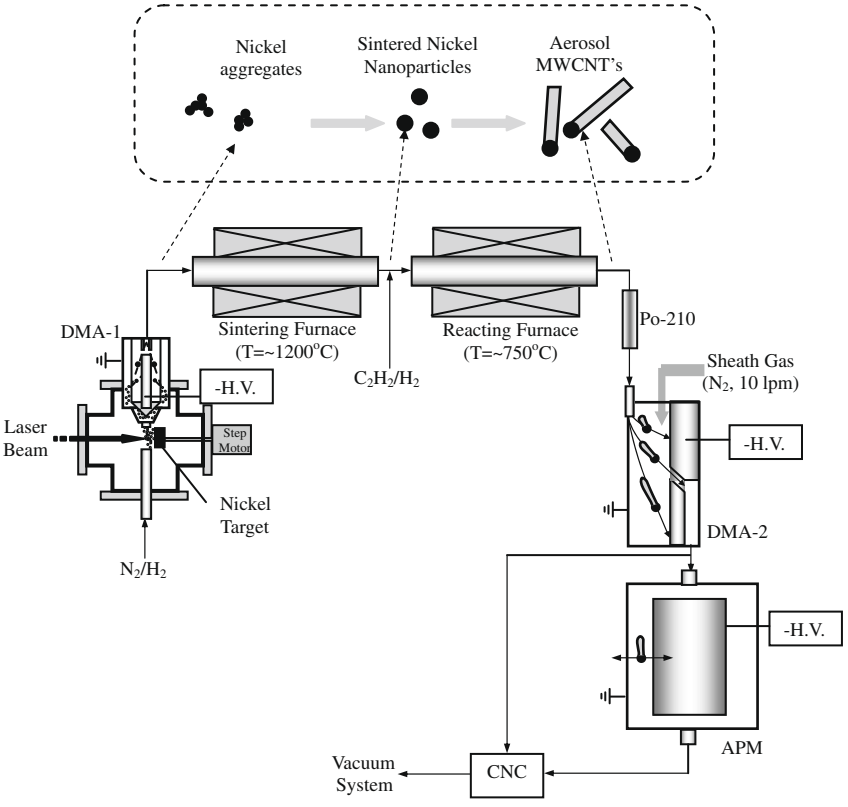

Fig. 1 – Schematic of experimental system with laser ablation chamber to create catalyst particles, DMA-1 to size select catalysts, sintering furnace to make catalysts spherical, reacting furnace to grow MWCNT's, Po-210 radiation source to charge MWCNT's, DMA-2 and APM for length and mass measurements, and CNC to count MWCNT's.

While TEM analysis is used to determine the constants, the values of $A_{p,DMA}$ obtained in this study are obtained from the DMA using Eq. (3) above. From the A_{pCNT} obtained from Eq. (4) and the CNT diameter via the TEM, the volume and length of the CNTs are determined using the following equations:

$$V_{CNT} = \frac{\pi D_{CNT} A_{pCNT}}{4} \quad (4)$$

$$L_{CNT} = A_p / D_{CNT} \quad (5)$$

Here it is noted that the diameter of hollow core inside the CNTs is observed to be less than ~3 nm, which is much smaller than the outer diameter of CNTs. The ratio of the hollow core volume to the total CNT's volume is less than ~4%. Therefore the total volume of CNTs was evaluated without considering the volume of hollow core structure inside the nanotubes.

The mass distributions of the CNTs were measured using an APM (Ehara et al. [6]) consisting of two concentric electrodes rotated at a controlled speed. The electric force acting on a singly charged particle acts in one direction and the centrifugal force in the opposite direction. If these two forces are balanced, the CNTs will pass through the APM and be counted by a condensation nucleus counter (CNC), in which a nominal 8 μm droplet is grown from each CNT by the condensation of alcohol vapor. The droplet flow is aerodynamically focused and each droplet is counted via light scattering in the CNC (Hinds [7]). The equation expressing the balance of the two forces is given by:

$$mr\omega^2 = \frac{nV_{APM}}{r\ln(r_2/r_1)}, \quad (6)$$

where m is the particle mass, ω is the APM angular speed in rad/s, n is number of elementary units of charge, e is the elementary electrical charge, V_{APM} is the applied voltage, r_1 and r_2 are the radii of inner and outer electrodes (where, $r_1 = 9.95$ cm and $r_2 = 10.25$ cm), and r is the radial location of the particle approximated as $r = (r_1+r_2)/2$.

The accuracy of the APM was assessed by measuring the mass distribution of monodisperse aerosols made up of NaCl and of dioctylphthalate (DOP). The particle diameters of the spherical particles were 50, 100, and 150 nm (or 200 nm). The particle diameter was determined using the following relationship between the electrical mobility of a singly charged particle and particle diameter:

$$Z_m = \frac{eC(D_p)}{3\pi\mu D_p}, \quad (7)$$

where $C(D_p)$ is the Cunningham slip correction given by (Hinds [7]):

$$C(D_p) = 1 + \frac{\lambda}{D_p}\left(2.34 + 1.05\exp\left(-\frac{0.39D_p}{\lambda}\right)\right) \quad (8)$$

The particles exiting have a peak diameter determined from Eqs. (1) and (8) and the standard deviation of the size distribution is slightly more than 2% of the peak diameter for the case where the ratio of the sheath flow to aerosol flow is 10 to 1.

The results for the average mass and the computed average density for each particle size are presented in Table 1. It is seen from the Table 1 that the nominal deviation between the measured density and the known density for DOP and NaCl is about 4%. We use this as a measure of the relative uncertainty in the mass measurement by the APM.

A key to measuring the density of CNTs using the DMA and APM is the generation of nanotubes with nearly the same diameter and length. This was done by the combination of mobility classification of nickel particles and a thermal CVD process. The aerosol exiting the central electrode of the DMA has a narrow mobility distribution compared to the inlet aerosol and is said to be classified. For a sheath flow to aerosol flow ratio of ten, the standard deviation of the mobility distribution for the CNTs exiting the electrode is 4% of the mean mobility. The approximately factor of two smaller standard deviation for the diameter distribution results from the Cunningham slip correction being inversely proportional to particle diameter in the small particle limit. A polydisperse nickel catalyst nanoparticle aerosol was generated by a pulsed laser ablation system using a 1064 nm Q-switched Nd:YAG laser operating at 10 Hz with a pulse width of 4 ns. The nanoparticles were each clusters of several spherules. The nickel nanoparticles were mobility-classified by DMA-1 operating at 1 Lpm of nickel particle-laden flow and 10 Lpm of nitrogen sheath gas (see in Fig. 1), and then they were annealed in a tube furnace reactor (2.5 cm dia. × 60 cm heating length) to yield spherical-like monodisperse particles after a 3 s residence time at 1200 °C. The annealed nickel nanoparticles then were mixed with acetylene and hydrogen in a second tube furnace (2.5 cm dia. × 50 cm heating length) at ~700 °C resulting in the growth of free-flight CNTs. The as-grown free-flight CNTs had a nearly uniform diameter, as a result of the monodispersity of the nickel catalyst, and a wide range of lengths. The CNTs were passed through a bi-polar distribution of ions produced by α radiation from Po^{210}. This resulted in primarily singly charged CNTs, which were subsequently introduced into the DMA-2 for further classification based on electrical mobility. The DMA-2 combined with a CNC was used to measure the mobility distribution of the CNTs.

Fig. 2 presents the results of tandem DMA measurement showing the effect of the acetylene reaction on the size distribution of mobility-selected nickel particles. The applied voltage in DMA-1 was chosen such that the geometric mean diameter (GMD) of initial nickel particles were ~15 and ~22 nm with corresponding projected areas of about 180 and 380 nm^2. It is also found that the fiber diameters measured by TEM analysis is within 1 nm of the GMD of the catalyst particle. As one can see, both peaks of nickel particles disappeared after they reacted with controlled amounts of acetylene and hydrogen, indicating that the growth of CNTs were mediated by the presence of nickel particles. The two broad distributions with mean equivalent mobility diameter of ~90 and ~100 nm, corresponding to projected areas of about 8000 and 10,000 nm^2, are for free-flight CNTs. The mobility diameter is the diameter of a sphere with the same mobility as the CNT and is obtained from Eq. (7).

The second DMA classifies the CNTs in terms of length. These as-grown CNTs (see Fig. 1) classified by the DMA-2 were subsequently introduced into the APM, which was operated at a fixed rotational speed (~3000 RPM) and with a ramped applied voltage to classify the CNTs based on their mass. The number concentration of CNTs exiting the APM was counted by a CPC at the outlet of the APM. Fig. 3 presents the mass dis-

Table 1 – Summary of absolute material density of DOP and NaCl particles measured by tandem DMA–APM system.

Material	Mobility diameter (nm)	Spherical particle volume V_p (cm^3)	Mass peak measured by APM, M_p (fg)	ρ_p (g/cm^3)	Error (%)
DOP	50	6.54×10^{-17}	0.069	1.055	+7.0
	100	5.24×10^{-16}	0.531	1.013	+2.8
	200	4.19×10^{-15}	4.223	1.008	+2.2
NaCl	50	6.54×10^{-17}	0.150	2.294	+5.9
	100	5.24×10^{-16}	1.104	2.107	−2.7
	150	1.77×10^{-15}	3.703	2.092	−3.4

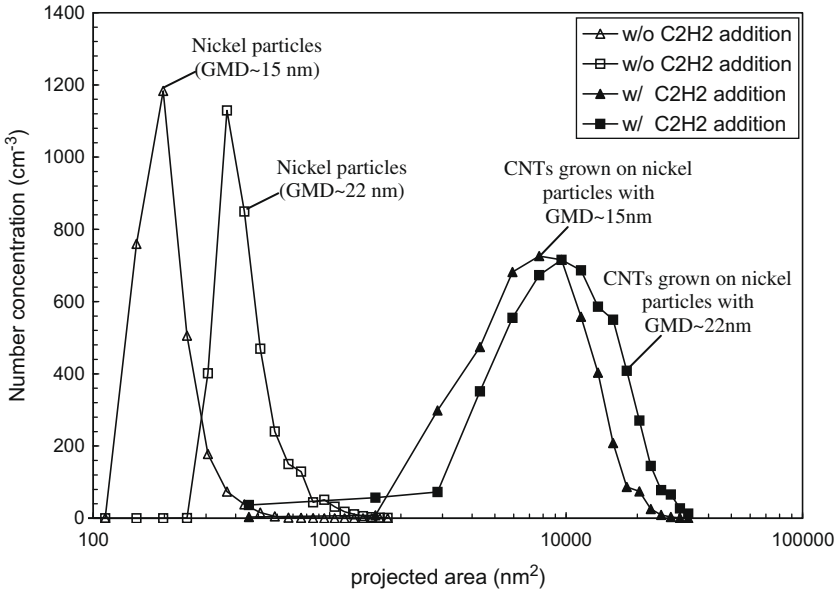

Fig. 2 – The evolution of mobility size distributions of size selected nickel nanoparticles with and without hydrocarbon (i.e. C_2H_2) reaction for growing CNTs.

tributions of CNTs classified by the DMA-2 operated at fixed mobility sizes of 70, 100, and 130 nm, respectively. The peak mass of each free-flight CNTs is given in Table 2. As one can see in Fig. 3a, CNTs classified at a larger mobility size have a larger mass distribution, implying that longer nanotubes are classified at a larger mobility size. To see the effect of CNT's diameter on the mass distributions, we produced free-flight CNTs with a diameter of ~22 nm. As seen in Fig. 3b, the average mass of CNTs with larger diameter (i.e. D_{CNT} = 22 nm) is greater than the average mass for the CNTs with smaller diameter (i.e. D_{CNT} = 15 *nm, see Fig. 3a*).

Table 2 summarizes the calculation procedure for determining the nanotube's density. Since the CNTs are grown on each seeded-nickel particle, it is noted that the average mass of resulting materials measured by tandem DMA–APM system in our approach presents the summation of mass of pure CNT (i.e. M_{CNT}) and mass of seeded Ni particle (i.e. M_{Ni}). As such, the mass of each catalytic nickel particle with a known mobility size (i.e. D_{Ni} = 15 or 22 nm) and bulk density (ρ_{Ni} = 8.9 g/cm^3) is subtracted from the peak mass of nanotube/catalytic composite particle measured by tandem DMA–APM system. From TEM analysis it is found that there is a single Ni catalyst particle associated with each CNT. As one can see, the mass contribution of seeded-nickel particle increases as the nanotube length decreases and the diameter of seeded particle increases. After making this mass correction, the density of CNTs is calculated by taking the ratio of the mass of pure CNT (M_{CNT}) to the volume of CNT (V_{CNT}) which is corrected for the volume of the Ni catalyst. The average density of CNTs (ρ_{CNT}) is found to be 1.74 ± 0.03 g/cm^3 (where, $\rho_{CNT} \pm \sigma/\sqrt{n}$, where σ is the standard deviation of the six measurements and n is the number of measurements).

The density for the two groups of CNTs with the diameter of 15 and 22 nm, respectively, are also found to be similar. One might expect a near constant density for CNTs with this range of diameters, since a diameter of 15 nm corresponds to about 20 graphite layers.

For both the 15 and 22 nm diameter CNT there is a systematic decrease in the particle density by about 9% as the length increases by about a factor of 4. One possible explanation of this effect is that the relationship between A_{pCNT} and $A_{p,DMA}$ is slight non-linear. This would lead to a systematic dependence of density on CNT length.

The standard deviation of the six density measurement is about 4%; however, the combined uncertainty is larger. We estimate the uncertainties in the measurements of D_{CNT},

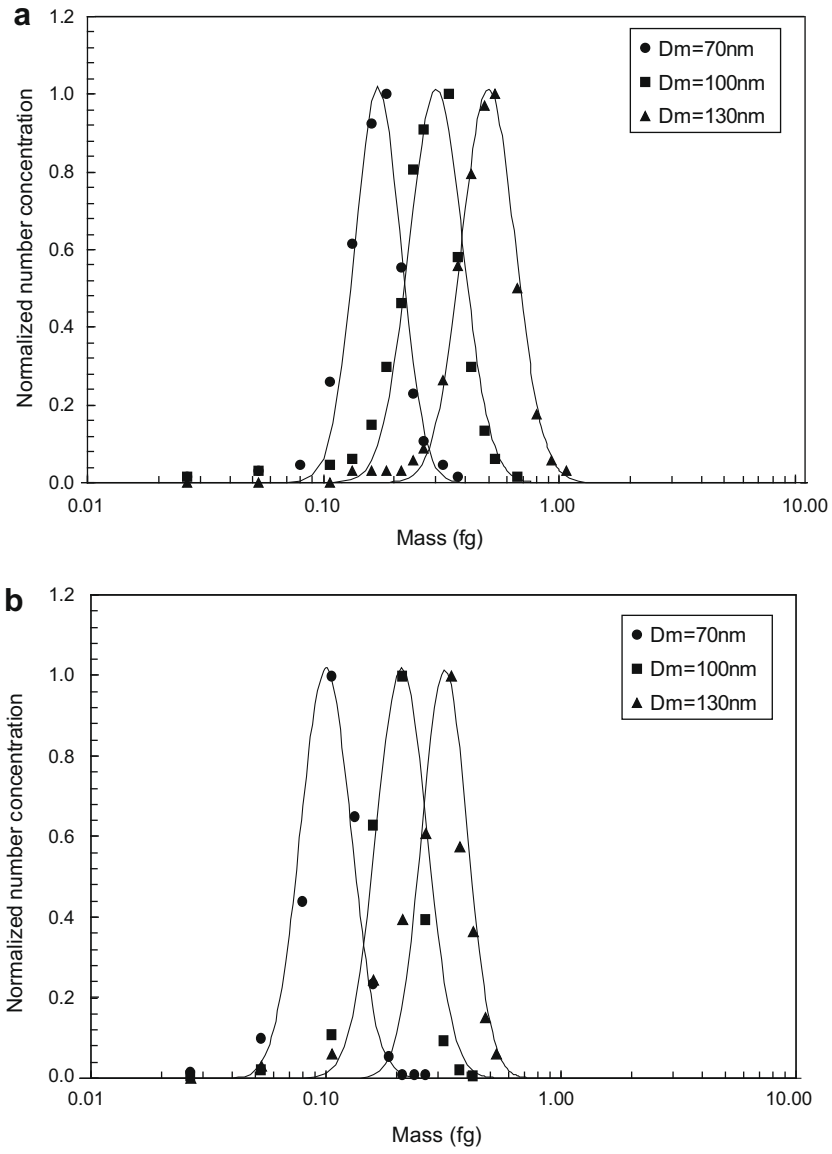

Fig. 3 – Mass distributions of mobility-classified CNTs with the diameter of (a) D_{CNT} = 15 nm and (b) D_{CNT} = 22 nm (solid lines are the lognormal Gaussian curves fitted into the APM measurement data marked with solid symbols).

A_{pCNT}, and the mass to be ±5%, ±7%, and ±4%. The following expression for the density is used for the uncertainty propagation:

$$\rho_{CNT} = \frac{4M_{CNT}}{\pi D_{CNT} A_{pCNT}} \tag{9}$$

The resulting combined uncertainty for density is found to be ±9% so that the density is (1.74 ± 0.16) g/cm^3. This density is significantly lower than graphite, 2.22 g/cm^3. The densities of nine different amorphous carbon blacks measured by helium pyncnometry vary from 1.84 to 2.06 g/cm^3 (Donnet and Voet [8]) and the average value of 1.94 is outside the uncertainty range for our measurements. So the density of CNTs appears to be lower than other forms of carbon.

One possibility is a large hollow core. One finds that the diameter of the hollow core would need to be about half the overall diameter if the density of the nanotube condensed phase was equal to that of graphite. As discussed above, the TEM data does not indicate such a large hollow core.

Another possibility is that the diameter of the CNT has been overestimated. If the diameter were 13.1 nm rather than 15 nm, then the estimated density would be equal to that of graphite. It is possible that the diameter has been underestimated, but 1.9 nm exceeds the 2 sigma uncertainty in the diameter measurement. Having eliminated these two possibilities, we are left with the conclusion that the density of these free-flight multiwalled CNTs, (1.74 ± 0.16) g/cm^3, is significantly lower (about 3 sigma) than for graphite and is about 1 sigma lower than the average of the density measurements for carbon black. We are not aware of any other density measurements for mulitwalled CNTs produced by a gas phase process.

Table 2 – Summary of absolute material density of CNTs measured by tandem DMA–APM system.

D_{CNT} [nm]	D_m [nm]	[a]$A_{p,DMA}$ [nm^2]	[b]A_{pCNT} [nm^2]	[c]L_{CNT} [nm]	[d]V_{CNT} [nm^3]	[e]V_{Ni} [nm^3]	[f]M_{Ni} [fg]	[g]M_{CNT+Ni} [fg]	[h]M_{CNT} [fg]	[i]ρ_{CNT} [g/cm^3]
	70	3208	4121	275	48,546	1767	0.016	0.101	0.084	1.796
15	100	5931	9042	603	106,523	1767	0.016	0.200	0.184	1.756
	130	9711	15,872	1058	186,993	1767	0.016	0.322	0.304	1.641
	70	3208	4121	187	71,201	5575	0.050	0.169	0.120	1.829
22	100	5931	9042	411	156,234	5575	0.050	0.308	0.260	1.726
	130	9711	15,872	721	274,256	5575	0.050	0.501	0.450	1.675

a $A_{P,DMA}$ from Eq. (2).
b $A_{pCNT} = L_{CNT}D_{CNT}$ from Eq. (3).
c $L_{CNT} = \frac{A_{pCNT}}{D_{CNT}}$.
d $V_{CNT} = \frac{\pi}{4}D_{CNT}A_{pCNT}$(i.e. cylindrical shape), volume of Ni particle not included.
e $V_{Ni} = \frac{\pi}{6}D_{Ni}^3$ (where, $D_{Ni} = D_m$).
f $M_{Ni} = V_{Ni}\rho_{Ni}$ (where, $\rho_{Ni} = 8.9$ g/cm^3).
g M_{CNT+Ni} is the peak mass of mobility-classified CNTs with seeded-nickel particle measured by APM and is obtained by Gaussian fits to the mass distribution curves in Fig. 3.
h $M_{CNT} = M_{CNT+Ni} - M_{Ni}$.
i $\rho_{CNT} = \frac{M_{CNT}}{V_{CNT}}$.

3. Conclusions

In this paper we have developed an on-the-fly approach to measure the density of MWCNT's. More generically we also point out that the tandem DMA–APM technique described in this work enables one to make real-time measurements of the density of nanoscale elongated non-spherical materials with high aspect ratio (e.g. nanowires, nanofibers, or nanotubes), which have masses down to sub-femtograms.

REFERENCES

[1] Park K, Kittelson DB, Zachariah MR, McMurry PH. Measurement of inherent material density of nanoparticle agglomerates. J Nanoparticle Res 2004;6(2):267–72.

[2] Kim SH, Liu BYH, Zachariah MR. Method for measuring the charge and size distribution of nanoaerosols. J Colloid Interface Sci 2005;282(1):46–57.

[3] Knutson EO, Whitby KT. Aerosol classification by electric mobility: apparatus, theory, and applications. J Aerosol Sci 1975;6(6):443–51.

[4] Kim SH, Mulholland GW, Zachariah MR. Understanding ion-mobility and transport properties of aerosol nanowires. J Aerosol Sci 2007;38:823–42.

[5] Kim SH, Zachariah MR. In-flight kinetic measurements of the aerosol growth of carbon nanotubes by electrical mobility classification. J Phys Chem 2006;110:4555–62.

[6] Ehara K, Hagwood C, Coakley KJ. Novel method to classify aerosol particles according to their mass-to-charge ratio-aerosol particle mass analyser. J. Aerosol Sci 1996;27(2):217–34.

[7] Hinds WC. Aerosol technology: properties, behavior, and measurement of airborne particles. New York, NY: John Wiley and Sons, Inc.; 1999. p. 48–51.

[8] Donnet J, Voet A. Carbon black: physics, chemistry, and elastomer reinforcement. Marcel Dekker, Inc.; 1976. p. 147–51.